Induced Flow Variation of the Helicopter Rotor Operating in the Vortex Ring State

AKIRA AZUMA* AND AKIRA OBATA†
University of Tokyo, Tokyo, Japan

By using small, quickly responsive, and very sensitive windmills we can measure the inflow variation of the model-helicopter rotor operating in the vortex ring state. The wind-tunnel tests show that 1) as the rotor starts to descend vertically, the periodic-induced-flow variation is observed at the rotor tip without any notable thrust change; 2) when the rate of descent approaches the induced velocity generated at hovering state, a thrust reduction appears, this being closely correlated with the increment of the downwash component near the rotor tip induced by a strong vortex ring; 3) as the rate of descent increases beyond the aforementioned induced velocity, the downwash variation becomes predominant near the center of the rotor and the thrust variation tends to decrease; 4) torque variation is not observable for low collective pitch operation, but for high pitch the torque fluctuates with thrust variation. The preceding final result is explained by the blade element theory with measured inflow.

Nomenclature

a = lift slope of the rotor blade
b = number of blade
c = chord of the rotor blade
c_0 = root chord of the blade
e = radius of blade cut out
Q = torque
$\bar{Q}$ = mean torque
ΔQ = fluctuation of torque $= Q - \bar{Q}$
r = radius of the blade element
r_i = radial distance of the anemometer at the ith station
R = rotor radius
S = disk area $= \pi R^2$
T = thrust
$\bar{T}$ = mean thrust
ΔT = fluctuation of thrust $= T - \bar{T}$
v_i = inflow velocity through the disk at the ith station (positive to downwash direction)
$\bar{v}_i$ = mean inflow velocity at ith station
Δv_i = inflow fluctuation at the ith station $= v_i - \bar{v}_i$
$v_i(t)v_j(t+\tau)$ = correlation function of two variables $v_i(t)$ and $v_j(t+\tau)$
$$v_j(t+\tau) = \lim_{T\to\infty} \frac{1}{2T}\int_{-T}^{T} v_i(t)v_j(t+\tau)dt$$
v_h = mean induced velocity at hovering state $= (T_h/2\rho S)^{1/2}$
V = rate of descent
x_i = r_i/R
Z = distance from rotor disk to anemometer (positive to the downwash direction)
α = angle of attack of the rotor disk
$\delta_0, \delta_1, \delta_2$ = blade drag coefficients
θ = blade pitch
θ_r = blade pitch at root
λ_r = inflow angle $= v/(r\Omega)$
ρ = air density
ρ_{ij} = normalized correlation function
$$= [\overline{v_i(t)v_j(t+\tau)} - \overline{v_i(t)}\,\overline{v_j(t+\tau)}]/\{[\overline{v_i(t)^2} - \overline{v_i(t)}^2][\overline{v_j(t)^2} - \overline{v_j(t)}^2]\}^{1/2}$$
for instance, ρ_{ab} means the cross correlation of v_a and v_b
ρ_{TT} = normalized autocorrelation function of thrust fluctuation
σ = solidity $= bc/\pi R$
τ = time, sec
ψ = azimuth angle
Ω = rotational velocity of the rotor

Subscripts

h = hovering state
rms = root mean square

Introduction

POWER-ON, especially vertical, descent flight has recently been of considerable engineering interest for multiengine helicopters operating in confined urban sites or over congested areas in which emergency landing sites are not available. The performance of a helicopter in vertical flight cannot, however, be predicted by simple momentum theory over a range of vertical or near-vertical descent in which the rotor is surrounded by a vortex of turbulent air.

Such vortex ring state has been observed by smoke test in wind tunnel,[1] and flight experiences.[2,3] Further, the empirical relation between induced power and rate of descent of the rotor has been determined by wind tunnel tests[4–9] and flight tests.[2,3] Although the vortex ring state is characterized by unsteady or turbulent flowfield around the rotor, the past experiments have been confined to measuring the mean induced power for a given rate of descent.

Yaggy et al.[10] and a group including one of the present authors have given attention to the unsteady aerodynamic characteristics of the rotor operating in the vortex ring state, and the latter has succeeded in measuring the thrust and torque oscillations of the rotor.[11,12] It was observed from the aforementioned tests that in the vortex ring state the thrust oscillation was pronounced and its periodicity was predominant at oblique descent ($\sigma = 60°$–$70°$) rather than vertical descent ($\alpha = 90°$).

In order to investigate the reason why the thrust oscillation is more severe than the torque variation, simultaneous measurement of the induced flow, or more precisely of inflow,‡ through the rotor disk with the thrust and torque is attempted, and a range of torque variation with respect to the thrust is determined by the blade element theory.

Received October 16, 1967; revision March 5, 1968.

* Associate Professor, The Institute of Space and Aeronautical Science. Member AIAA.
† Graduate Student, Department of Aeronautical Engineering.

‡ Here, the inflow is considered as a summation of the induced flow generated by the vortex systems and the upflow due to the rate of descent.

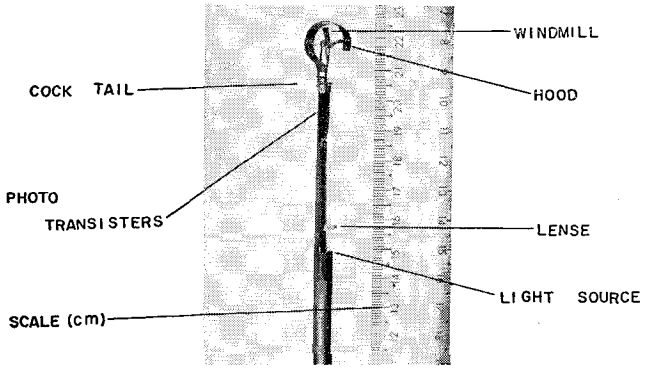

Fig. 1 Windmill anemometer.

Windmill Anemometer

For measuring the inflow variation of the model helicopter rotor operating in the vortex ring state, the anemometer that can measure the speed range from -2 to $+5$ m/sec and frequencies of less than 1 cps will be required. It should, however, be noted that the hot-wire anemometer is delicate and primarily suitable to detect high-frequency-velocity fluctuations generated by small vortices, and hence may not be suitable for investigating the whole flowfield of the rotor operating in the vortex ring state. On the contrary, it may be difficult or impossible for the Pitot-static tube to detect such low and fluctuating wind velocity.

It will be considered that the windmill anemometer is a proper instrument to match the preceding requirements if the anemometer has good response characteristics. We have, therefore, developed such windmills (see Fig. 1) which have the following characteristics: 1) small size and light weight (do not appreciably disturb the flow pattern and due to low inertia), 2) high rotational speed (retains high accuracy with low wind velocity), and 3) maintains sensitivity through wide variations in yaw angles.

The windmill developed to have the aforementioned characteristics comprises a hood or shroud and four blades made of aluminium foil which are secured to the hollow aluminium tube which is, in turn, journaled to crystal bearings supported at the ends of U-arms, a weathercock made of balsa and two photo-transistors attached to a stem with a lense and a light source as shown in Fig. 1. Each blade reflects the light from the source to either of the two transistors, one of which is blinded by a plate secured to an opposite arm of the weathercock which is pivotally supported on the top of stem with U-arms. The photo-transistor triggered by the light sends pulses to an amplifier in which each pulse is rectified and amplified, and then a current corresponding to a certain rpm of the windmill is generated. When the wind direction is reversed, the photo-transistor which has been blinded in the normal wind will be opened for light and the other will be blinded by the plate of the weathercock so that the output of the former transistor will be set to produce negative current and the reversal of the wind direction will be able to detect.

The present windmill anemometer has the following satisfactory characteristics: By running the windmill anemometer mounted on a carriage which can be run on tracks with any given exact speed from 0–10 m/sec we have confirmed that the complete windmill anemometer has good linearity for either normal or reverse wind direction. Figure 2 shows the time response for step input of the wind velocity, which is obtained by entering the anemometer quickly into the air jet or quickly removing it. As seen from the Fig. 2, the time constant of this windmill anemometer assembly may be estimated about 0.3 sec in which the time constant of the amplifier is regarded to be about 0.14 sec. Figure 3 shows the effect of yaw angle on the windmill. With the hood, the accuracy is unimpaired through wide variation in yaw angles, particularly in the normal wind direction.

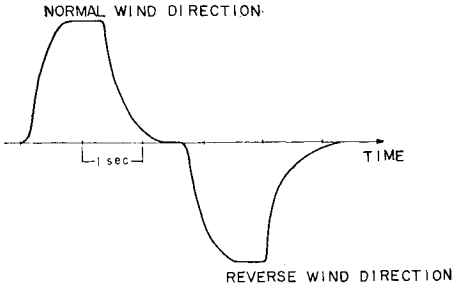

Fig. 2 Response curve for step input.

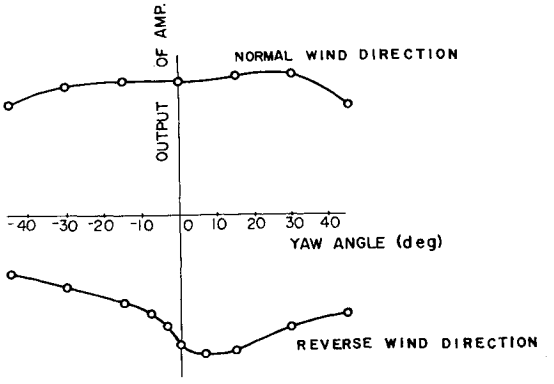

Fig. 3 Effect of yaw angle.

Model and Apparatus

A model rotor to be tested is arranged in 3-m-diam wind tunnel as shown in Fig. 4. The rotor is driven by a d.c. motor about 1000 rpm. The rotor has three blades made of aluminum which can flap and lag. The geometrical properties of the rotor are as follows: the diameter is 1100 mm, the solidity is 0.0573, the blade section is NACA 0012, and either twisted ($-8°$ from root to tip) or untwisted blades have been used for the test.

The windmills are arranged as shown in Fig. 5. Torque and thrust are measured through strain-gage-balance systems which are supported under the hub of the rotor, and the data are recorded simultaneously on a recording oscillograph with the outputs of the windmill anemometers. The rotors were tested under the following conditions: descent angle was 90°, rotational speed was about 1000 rpm, rate of descent was from 1 to 5 m/sec, and the blade pitch at root was from 8–22°.

Inflow Pattern in the Vortex Ring State

A typical example of the data obtained during the tests is shown in Fig. 6 in which T and Q are thrust and torque of the rotor and v_1 through v_{10} are inflow velocities at each radial station through the rotor disk, respectively. As seen from Fig. 6, the most distinctive feature on the rotor having twisted blades in the region of the vortex ring state is the violent thrust fluctuation. This thrust fluctuation seems to cor-

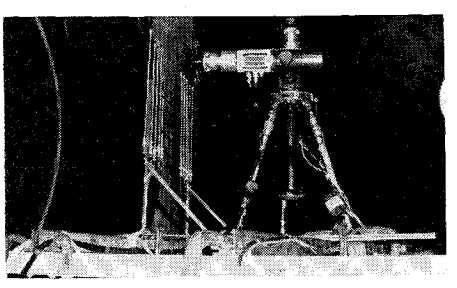

Fig. 4 Experimental apparatus.

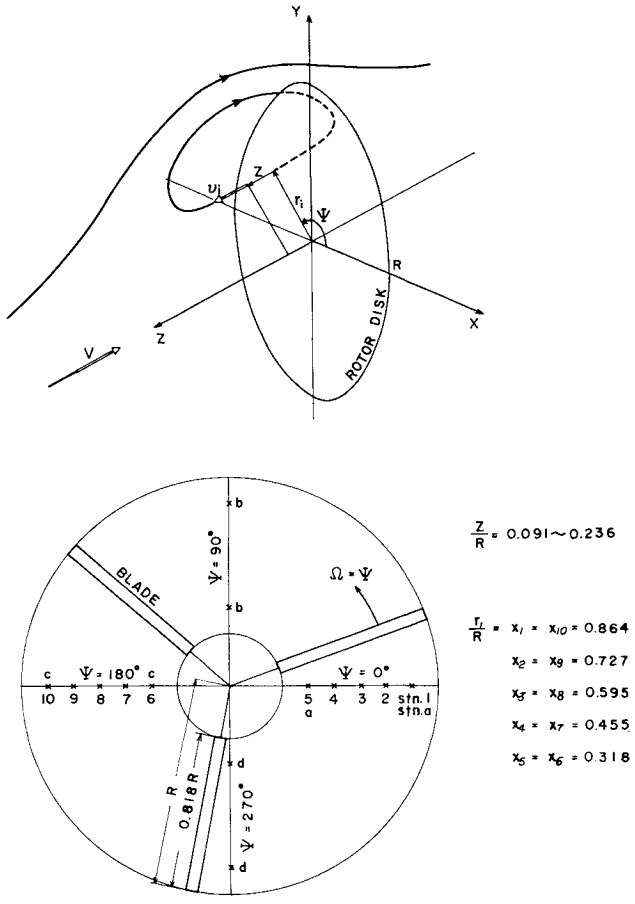

Fig. 5 Windmills arrangement.

relate with the inflow through the rotor, specifically near the tip region. This is demonstrated in Fig. 7 which a) shows the location of the measured inflow, b) shows the thrust variation from that of hovering state vs whole summation of the inflows, and c) shows the same thrust variation vs inflows near tip region of the rotor. The data obtained in b) a little more scattered than those of c). It is very interesting to note that the strong inflow near the tip region, which must be generated by a vortex ring near the rotor tip, decreases the thrust appreciably.

As the rate of descent increases several flow patterns of the inflow are observed. Figure 8 shows such patterns of the inflow variation with respect to the rate of descent nondimensionalized by the induced velocity and rotor speed at hovering state.§ As shown in a) of Fig. 8, the inflow variation is

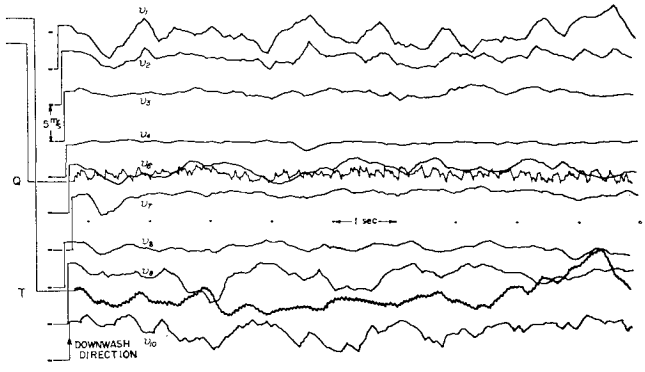

Fig. 6 A typical test result for twisted blade, $\alpha = 90°$, $\theta r = 12°$, $V\Omega_h/v_h\Omega = 0.83$, $Z/R = 0.236$.

§ In Refs. 11 and 12, a more simple nondimensional form, i.e., V/v_h or $V/R\Omega$, has been adopted; it must, however, be pertinent to use the form $(V/v_h)(\Omega_h/\Omega)$ for the present purpose.

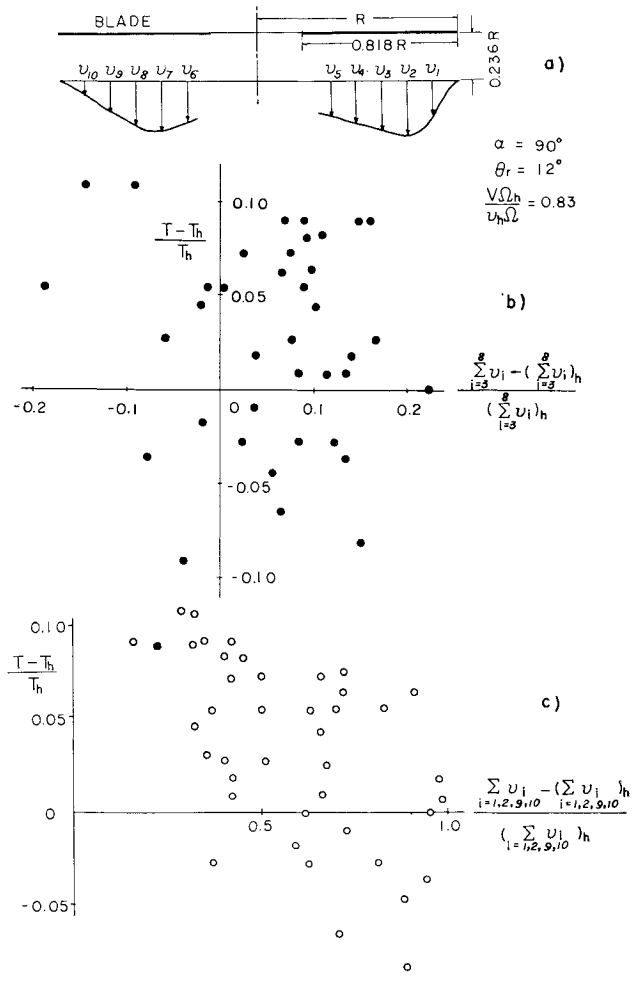

Fig. 7 Correlation between induced flow and thrust for twisted blade.

mainly observed near the tip region in the range of $(V/v_h) \times (\Omega_h/\Omega) \leqq 0.8$. At a certain instant, the inflow distribution in a plane through the hub takes the form defined by the solid line; then, in the next step, the distribution will change to another form defined by the dotted line. The most severe inflow fluctuation is observed at $(V/v_h)(\Omega_h/\Omega) \fallingdotseq 0.8$. As the rate of descent approaches the induced velocity at hovering state, $1.2 > (V/v_h)(\Omega_h/\Omega) > 0.8$, the region in which the inflow fluctuates shifts from the tip side to the root side of the rotor as shown in b of Fig. 8, and the thrust oscillation decreases rapidly. For still higher rates of descent, $(V/v_h)(\Omega_h/\Omega) \fallingdotseq 1.2$, as shown in c) of Fig. 8 the up-flow due to the large rate of descent overcomes the induced flow and tends to penetrate near the root. It is interesting to note that the pene-

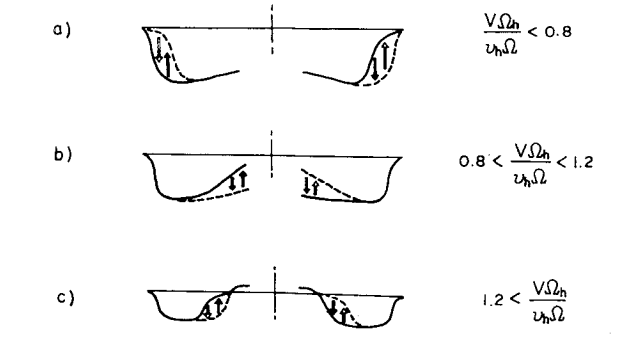

Fig. 8 Flow patterns appeared in the vortex ring state.

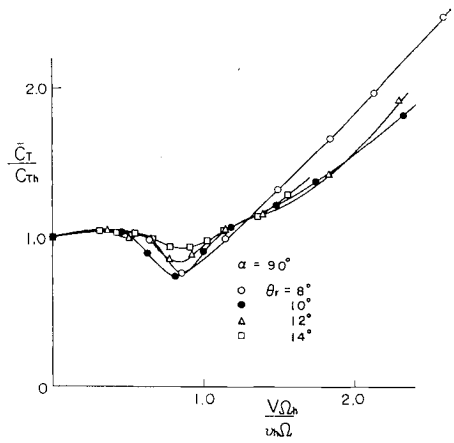

a) Continued

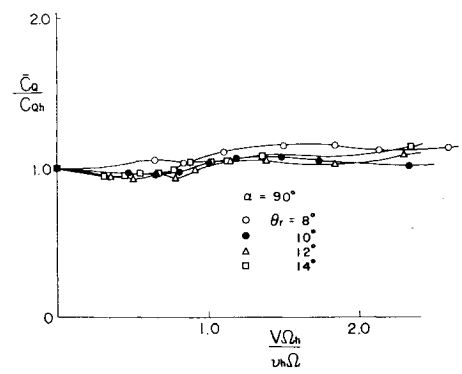

b) Continued

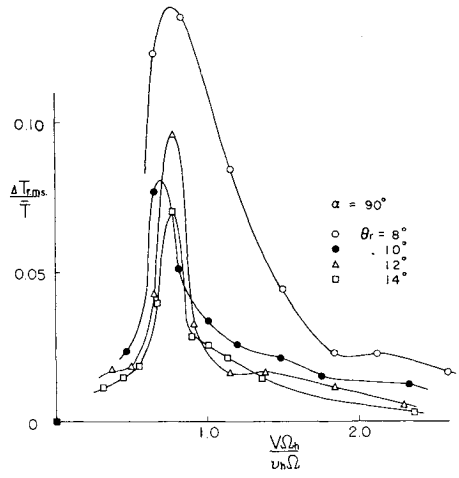

c) Continued

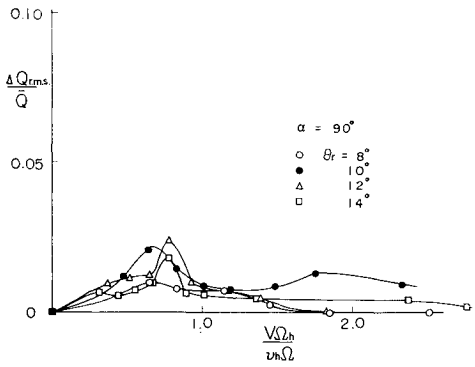

d) Concluded

Fig. 9 Thrust and torque characteristics versus nondimensional descent velocity for twisted blade.

trated portion near the rotor hub no longer fluctuates. Beyond this point, $(V/v_h)(\Omega_h/\Omega) > 1.2$, the flow around the rotor will change from the vortex ring state to the windmill brake state.

The preceding description is illustrated in Fig. 9 where a and b show the mean thrust and torque coefficients, respectively, vs the nondimensionalized descent velocity, and c and d show the root mean squares of the thrust and torque variation, respectively. The mean thrust reduction occurs at the $(V/v_h)(\Omega_h/\Omega) \fallingdotseq 0.8$ (see a) where the most severe thrust fluctuation is observed (see c). The figure does not indicate a similar variation in the torque.

The similar representation is shown in Fig. 10a for the mean inflow and b for the root mean square of the inflow fluctuation. The mean inflow velocity for each anemometer, except for the 1st anemometer, keeps an almost constant value until the rate of descent approaches $(V/v_h)(\Omega_h/\Omega) \fallingdotseq 0.8$ as shown in a of Fig. 10. The 1st anemometer is located just outside the contracted slip stream at the hovering state so that, as the rate of descent increases, the inflow near this point is detected by the anemometer. The inflow fluctuation of the tip side detected by no. 1 anemometer is larger than that of the root or inside of the rotor detected by 2nd $\sim$ 5th anemometers, within the small rate of descent range, $(V/v_h)(\Omega_h/\Omega) < 0.8$. Beyond this rate of descent, the inflow fluctuation of the inside becomes predominant as shown in b of the Fig. 10.

Figure 11 shows the auto- or cross correlations of the inflow velocities at four orthogonal points circumferentially located on Fig. 11a, $v/R = 0.86$, and Fig. 11b, $r/R = 0.32$. The auto-correlation of a is taken from the data obtained at the vertical descent of $(V/v_h)(\Omega_h/\Omega) = 0.593$. Around the preceding descent speed, the tip inflow fluctuation behaves periodically as seen from Fig. 11a and this periodicity ($\tau\Omega \fallingdotseq 800$) seems to be obtained from the regular rotation of a disturbance along the rotor operating direction. As the rate of descent increases and approaches $(V/v_h)(\Omega_h/\Omega) = 0.8$ at which the severe thrust fluctuation may be observed the periodicity of the tip inflow becomes indefinite. Beyond this point it becomes that the periodicity ($\tau\Omega \fallingdotseq 100$) of the inflow fluctuation is observed at the rotor inside as shown in the Fig. 11b.

Although the periodical thrust fluctuation has been observed for oblique descent ($\alpha = 60° \sim 70°$)[11] similar periodical fluctuation of the thrust is not recognized for vertical descent in spite of the periodic fluctuation of either tip or root inflow. This fact may also be gathered from the auto-correlation taken on the thrust fluctuation as shown in Fig. 12.

Thrust and Torque Variation

According to the blade element theory, the thrust and torque are approximately given by[13]

$$T = \frac{\sigma}{2}\rho S(R\Omega)^2 \int_e^R \left(\frac{r}{R}\right)^2 a(\theta - \lambda_r)\left(\frac{C}{C_0}\right) d\left(\frac{r}{R}\right) \quad (1)$$

$$Q = \left(\frac{\sigma}{2}\right)\rho S(R\Omega)^2 R \int_e^R \left(\frac{r}{R}\right)^3 (1 + \lambda r^2)\{\delta_0 + \delta_1\theta + \delta_2\theta^2 + (a\theta - \delta_1 - 2\delta_2\theta)\lambda r - (a - \delta_2)\lambda r^2\}\left(\frac{C}{C_0}\right) d\left(\frac{r}{R}\right) \quad (2)$$

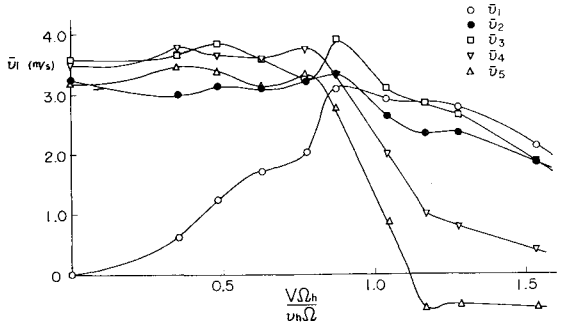

a) Continued

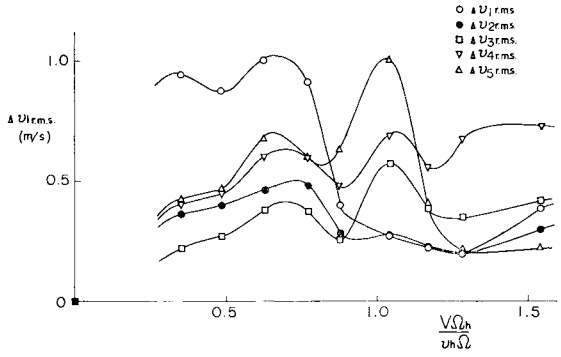

b) Concluded

Fig. 10 Inflow velocity characteristics for twisted blade; $\alpha = 90°$, $\theta r = 12°$, $Z/R = 0.182$.

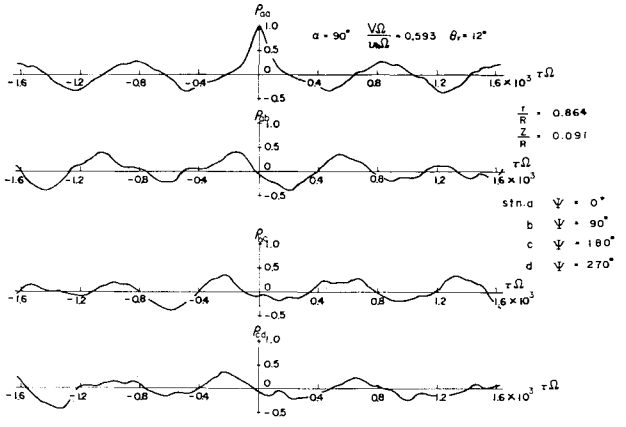

a) Continued

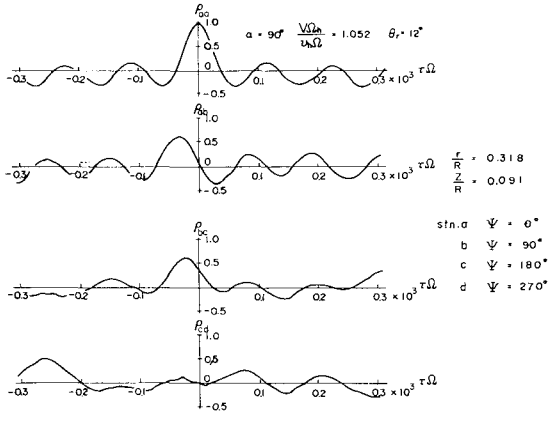

b) Concluded

Fig. 11 Auto- or cross correlations of the inflow velocities for twisted blade.

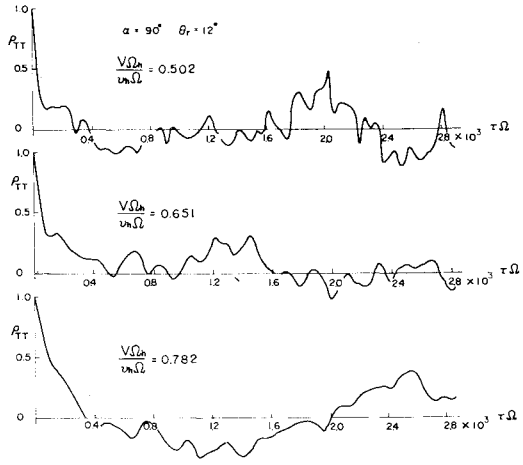

Fig. 12 Autocorrelations of thrust fluctuation or twisted blade.

In the vortex ring state, the local inflow angle may be assumed to take a value within the following range:

$$0 \leqq \lambda_r \leqq \theta \tag{3}$$

This is an expedient condition and imposes that, when $\lambda_r = \theta$ over the whole rotor disk, the thrust is nearly equal to zero and, when $\lambda_r = 0$, the windmill brake state initiates. The maximum and minimum inflow velocity distributions corresponding to $\lambda_r = 0$ and $\lambda_r = \theta$ are shown in Fig. 13 for twisted blades by solid lines. Measured inflow distribution in the vortex ring state is almost confined within the region defined by the solid lines as shown in Fig. 13.

Using the preceding assumption and Eqs. (1) and (2), the attainable range of thrust and torque will be calculated. Evidently, T/T_{max} can take any value between 0 and 1 for a given pitch angle but Q/Q_{max} is bounded considerably for given pitch angle. The possible ranges of the torque fluctuation for untwisted and twisted blades are given in Fig. 14, in which the torque can take values between $Q/Q_{max} = 1$ and each shaded line for a given pitch angle at the blade root. It is interesting to note that the possible torque fluctuation of the twisted blades is smaller than that of the untwisted blades

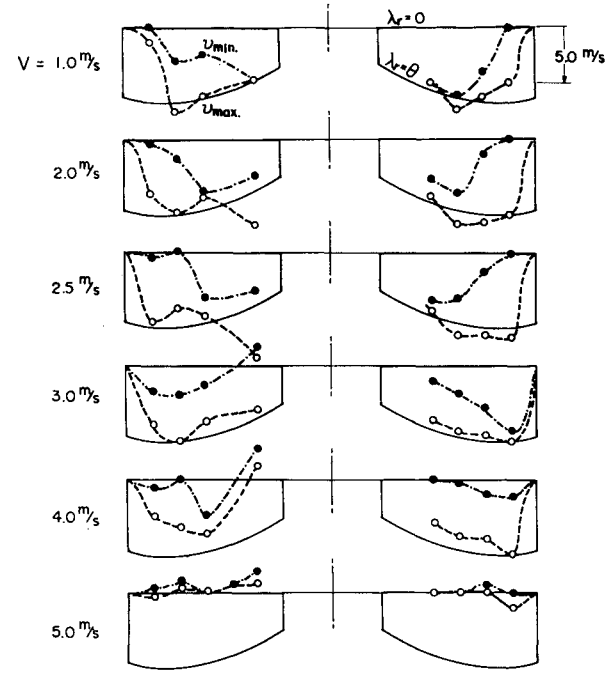

Fig. 13 Measured range of inflow distribution for twisted blade. $\theta_r = 14°$, 1000 rpm, $\alpha = 90°$; ○ measured maximum inflow velocity, ● minimum.

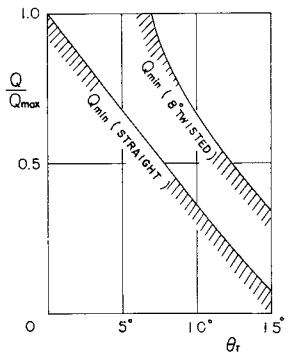

Fig. 14 Possible range of the torque fluctuation; α = 5.73, δ_0 = 0.0238, δ_1 = 0.0430, δ_2 = 0.716.

and in either blade configuration the fluctuation range decreases with small pitch angle instead of 100% thrust fluctuation.

From the preceding description it will be appreciated that a rotor having untwisted blades as well as the rotor having twisted blades operating with large pitch angle will experience the torque fluctuation with thrust. Figure 15 shows an example of oscillogram obtained for the rotor having untwisted blades. It is seen as expected that the torque, in this case, fluctuates with thrust.

Conclusion

By using windmill anemometers inflow fluctuation of the model-helicopter rotor operating in the vortex ring state have been measured. The results show the following characteristics.

The thrust reduction is closely related to the increment of the downwash component or inflow near the rotor tip induced by a strong vortex ring which appears when the rate of descent is nearly equal to the induced velocity generated in the hovering state. As the rate of descent increases beyond the induced velocity the inflow fluctuation becomes predominant near the rotor hub and the thrust variation tends to decrease. In this state the fluctuation shifts rotationally for the same direction of the rotor rotation. The torque variation is not observable for low collective pitch operation of the rotor having twisted blades but is recognized for high pitch operation, particularly for the rotor having untwisted blades. The preceding first and the last statements have been explained by the blade element theory with measured inflow distribution.

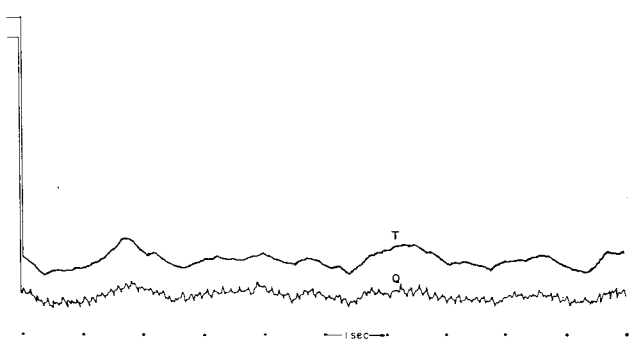

Fig. 15 A typical test result for untwisted blade. α = 90°, θ = 17°, V = 2.0 m/sec.

References

[1] Drees, J. M., Lucassen, L. R., and Jendal, W. P., "Airflow Through Helicopter Rotor in Vertical Flight," Rept. V. 1535, Dec. 1949, National Luchtvaart Laboratorium, Amsterdam.

[2] Stewart, W., "Flight Testing of Helicopters," *Journal of the Royal Aeronautical Society*, Vol. 52, No. 449, May 1948, pp. 261–304.

[3] Brotherhood, P., "Flow Through a Helicopter Rotor in Vertical Descent," R. & M. 2735, 1952, Aeronautical Research Council.

[4] Lock, C. N. H., Bateman, H., and Townend, H. C. H., "An Extension of the Vortex of Airscrews with Applications to Airscrews of Small Pitch, Including Experimental Results," R. & M. 1014, 1926, Aeronautical Research Council.

[5] Glauert, H., "The Analysis of Experimental Results in the Windmill Brake and Vortex Ring States of an Airscrew," R. & M. 1026, 1926, Aeronautical Research Council.

[6] Castles, W., Jr. and Gray, R. B., "Experimental Relation between Induced Velocity, Thrust and Rate of Descent of a Helicopter Rotor as Determined by Windtunnel Tests on Four Model Rotors," TN 2474, 1951, NACA.

[7] Lock, C. N. H., "Note on the Characteristic Curve for an Airscrew or Helicopter," R. & M. 2673, 1952, Aeronautical Research Council.

[8] Castles, W., Jr., "Flow Induced by a Rotor in Power-On Vertical Descent," TN 4330, 1958, NACA.

[9] Yaggy, R. F. and Mort, K. W., "Wind-Tunnel Tests of Two VTOL Propellers in Descent," TN D-1766, 1963, NASA.

[10] Stewart, W., "Helicopter Behaviour in the Vortex-Ring Conditions," R. & M. 3117, 1959, Aeronautical Research Council.

[11] Washizu, K. et al., "Experiments on a Model Helicopter Rotor Operating in the Vortex Ring State," *Journal of Aircraft*, Vol. 3, No. 3, May–June 1966, pp. 225–230.

[12] Washizu, K. et al., "Experimental Study on the Unsteady Aerodynamics of a Tandem Rotor Operating in the Vortex Ring State," *Proceedings of the 22nd Annual National Forum*, American Helicopter Society, Washington, D. C., May 11–13, 1966, pp. 215–220.

[13] Gessow, A. and Myers, G. C., Jr., *Aerodynamics of the Helicopter*, Macmillan, New York, 1952.